environmental microbiology

Environmental Microbiology (2019) **21**(7), 2375–2390 doi:10.1111/1462-2920.14622

Pseudomonas putida KT2440 metabolism undergoes sequential modifications during exponential growth in a complete medium as compounds are gradually consumed

Lázaro Molina,[1] **Ruggero La Rosa**,[2] **Juan Nogales**[1] **and Fernando Rojo**[1*]

[1]*Departamento de Biotecnología Microbiana, Centro Nacional de Biotecnología, CSIC, Madrid, Spain.*

[2]*Novo Nordisk Foundation Center for Biosustainability, Technical University of Denmark, Kgs. Lyngby, Denmark.*

Summary

***Pseudomonas putida* is a soil bacterium with a versatile and robust metabolism. When confronted with mixtures of carbon sources, it prioritizes the utilization of the preferred compounds, optimizing metabolism and growth. This response is particularly strong when growing in a complex medium such as LB. This work examines the changes occurring in *P. putida* KT2440 metabolic fluxes, while it grows exponentially in LB medium and sequentially consumes the compounds available. Integrating the uptake rates for each compound at three different moments during the exponential growth with the changes observed in the proteome, and with the metabolic fluxes predicted by the *i*JN1411 metabolic model for this strain, allowed the metabolic rearrangements that occurred to be determined. The results indicate that the bacterium changes significantly the configuration of its metabolism during the early, mid and late exponential phases of growth. Sugars served as an energy source during the early phase and later as energy and carbon source. The configuration of the tricarboxylic acids cycle varied during growth, providing no energy in the early phase, and turning to a reductive mode in the mid phase and to an oxidative mode later on. This work highlights the dynamism and flexibility of *P. putida* metabolism.**

Received 18 February, 2019; revised 2 April, 2019; accepted 4 April, 2019. *For correspondence. E-mail frojo@cnb.csic.es; Tel. (+34) 91 585 45 39; Fax (+34) 91 585 45 06.

Introduction

Pseudomonas putida KT2440 is a non-pathogenic, Gram-negative soil bacterium with many biotechnological applications (Poblete-Castro *et al.,* 2012). It has been certified as safe strain and approved for release into the environment (Fedral-Register, 1982). It is considerably resistant to harsh conditions, has a versatile and robust metabolism, is highly resistant to energetic stress and has low maintenance demands, all of which render this strain an ideal host organism for bioprocessing and for developing next generation synthetic organisms (Ebert *et al.,* 2011; Poblete-Castro *et al.,* 2012; Nikel *et al.,* 2014; Adams, 2016; Belda *et al.,* 2016). Although much is known about *P. putida* KT2440, its large genome (6.18 Mbp, Nelson *et al.,* 2002), its ability to use a wide range of compounds as carbon and energy sources and its sophisticated regulatory systems complicate the redirecting of its metabolism towards new functionalities. These properties pose particular challenges when trying to use the organism in bioremediation or biotransformation processes performed in complex growth media containing mixtures of carbon sources, such as waste biological materials.

When growing in complex media, pseudomonads use the available resources in a sequential and hierarchical manner, a process that is to a large extent orchestrated by the regulatory process termed catabolite repression (reviewed in Rojo, 2010). In this bacterial group, catabolite repression relies mainly on the Crc and Hfq regulatory proteins, the activities of which are controlled by small RNAs of the CrcZ family (Sonnleitner *et al.,* 2009; Moreno *et al.,* 2012; Moreno *et al.,* 2015; Sonnleitner *et al.,* 2018). The influence of this regulatory system is particularly strong in a complex media such as Lysogeny Broth (LB), which is a commonly used medium that allows high growth rates and has been thoroughly used to study the catabolite repression phenomenon. In this medium, the Crc/Hfq regulators influence both the order and the speed of assimilation of compounds available (Moreno *et al.,* 2009; La Rosa *et al.,* 2016). Catabolite repression not only inhibits the assimilation of a given compound until preferred ones have been

consumed, it fine-tunes the simultaneous assimilation of multiple compounds (del Castillo and Ramos, 2007; La Rosa *et al.,* 2016). In addition, the different concentrations of available compounds, the efficiency and/or expression of their transport systems, and/or the flux of metabolites through metabolic pathways might also contribute to define the hierarchy of their assimilation.

The sequential assimilation of the compounds in the LB during exponential growth suggests that cells continuously adapt their metabolism as preferred compounds are consumed and new ones start to be used. However, how *P. putida* gradually reorganizes its metabolic fluxes while growing exponentially in a rich medium such as LB has not been analysed in detail. To gain insight into this issue, the assimilation rates of LB components were determined during early, mid and late exponential growth. The data obtained were used to constrain the *i*JN1411 metabolic model for *P. putida* KT2440 and build a series of condition-specific models to provide the most probable flux distribution at each time point. The proteome of the cells at these same time points was analysed to help validating the fluxes predicted. Integrating these three approaches allowed identifying which metabolic pathways were used as cells consumed the different compounds in the medium. The results showed that the *P. putida* metabolic fluxes changed several times during growth, allowing the cells to constantly adapt to changing carbon and energy supplies without the need to stop growth to reprogram metabolic networks, as it occurs in other situations that give rise to a diauxic growth.

An interesting finding of this analysis is that the sugars present in the medium were consumed differently during the early, mid and late exponential phases of growth. *P. putida* KT2440 can use glucose, fructose and mannose as a carbon source but is not known to use polysaccharides (Sawyer *et al.,* 1977; Puchalka *et al.,* 2008; Dvorak and de Lorenzo, 2018). Glucose assimilation occurs through a cycle formed by enzymes of the Entner-Doudoroff, Embden-Meyerhof-Parnas and Pentose Phosphate pathways (del Castillo *et al.,* 2007, 2008; Nikel *et al.,* 2015). Glucose enters the periplasm via the OprB-I/OprB-II porins and may be directly transferred to the cytoplasm through an ABC transport system or be oxidized to gluconate in the periplasm by the periplasmic glucose dehydrogenase (Gcd). Gluconate can either be transported into the cell or be further oxidized to 2-ketogluconate in the periplasm by the gluconate dehydrogenase (Gad). The electrons detached from glucose or gluconate during oxidation in the periplasm are transferred to the ubiquinones of the cytoplasmic membrane, feeding the electron transport chain (Matsushita *et al.,* 1979; van Schie *et al.,* 1985). The cells can thus use glucose as an energy source without processing its carbon skeleton. The directly internalized glucose and 2-ketogluconate converge into 6-phosphogluconate, which is catabolized to pyruvate and glyceraldehyde 3-phosphate (G3P).

Earlier analyses have shown that *P. putida* catabolizes the different amino acids from LB in a hierarchical and sequential way (Moreno *et al.,* 2009; La Rosa *et al.,* 2016). Assimilation occurs through diverse pathways that, depending on the amino acid considered, eventually converge into pyruvate, acetyl-CoA or different intermediates of the tricarboxylic acids (TCA) cycle (Moreno *et al.,* 2009, and references therein). The results showed that the metabolic fluxes derived from the assimilation of these amino acids changed along the growth phase. All these findings highlight the flexibility and dynamism of *P. putida* metabolism.

Results

Composition of fresh LB

As a preliminary step, the composition of the fresh LB used in this work was determined; the results are indicated in Supporting Information Table S1 (column labelled 'Initial'). This medium is made from tryptone, that is, a tryptic hydrolysate of casein that provides amino acids and peptides, and yeast extract, which contains sugars, amino acids, peptides, organic acids, (poly)nucleotides, vitamins and micronutrients. The amino acids in LB can, therefore, either be free or form peptides of diverse length. Earlier analyses (La Rosa *et al.,* 2016) of the composition of LB showed free amino acids to be present at a total concentration of 26.8 mM, but those forming part of polypeptides were not detected by the technique used. In the present study, acid hydrolysis of the polypeptides of LB showed the total amino acid concentration to be 86.7 mM (Supporting Information Table S1). This compares well with the 99 mM reported by other authors (Sezonov *et al.,* 2007). Supporting Information Figure S1 shows the concentrations of free and total amino acids.

The LB medium is usually thought to include only scant quantities of carbohydrates (Sezonov *et al.,* 2007; La Rosa *et al.,* 2016). However, this idea derives from studies that used methods able to detect free sugars only, but not polysaccharides. The carbohydrates in LB derive from the yeast extract, which is a concentrate of the water-soluble fraction of autolysed *Saccharomyces cerevisiae* cells. The most abundant carbohydrates in this microorganism are trehalose (a disaccharide of glucose), polymers of glucose (glycogen and β-glucans) and polymers of mannose (mannan) (Aguilar-Uscanga and Francois, 2003; Plata *et al.,* 2013). The precise amount of carbohydrates in LB can vary according to the supplier used. In the present work, the total glucose content (free glucose plus that forming part of polysaccharides) was determined after an acid hydrolysis of the polysaccharides and found to be 14.6 mM

(in terms of glucose monomers; Supporting Information Table S1). Most glucose must be forming a part of polysaccharides, since free glucose in LB is present at 0.3 mM (La Rosa *et al.,* 2016). *P. putida* is unable to use polymers of mannose as a carbon source (see below); therefore, the concentration of this polysaccharide was not determined. Low-molecular-weight organic acids and (poly)nucleotides were also found in the LB used, although at smaller concentrations (Supporting Information Table S1).

Consumption of the compounds present in LB

P. putida KT2440 was inoculated into LB at a turbidity (A_{600}) of 0.05, and the composition of the medium analysed when the cells were in the initial stage of exponential growth (A_{600} of 0.2, after 2 h of growth), in mid exponential growth (A_{600} of 0.6, after 3 h of growth) and at the end of exponential growth (i.e., when cells were still actively growing but the growth rate had started to decline; A_{600} of 2, after 7 h of growth; Fig. 1A). The results showed that cells began growth by consuming acetate, succinate, formate, sugars and certain amino acids, mainly glutamine/glutamate (Supporting Information Table S1 and Fig. 1B and C; see also Fig. 2). Succinate, acetate, malate and formate were present at low concentrations and disappeared quickly, as previously reported (La Rosa *et al.,* 2016). Although *P. putida* KT2440 is not known to assimilate the polysaccharides present in LB, the concentration of glucose-polysaccharides decreased by 2 mM during the early exponential phase (labelled as 'total glucose' in Supporting Information Table S1; see also Fig. 1C). The disappearance of the sugars during the first 2 h of growth was paralleled by an increase in the concentration of 2-ketogluconate in the medium up to 2.6 mM (Fig. 1D); this compound was undetectable in the fresh LB at the start of growth. Since *P. putida* oxidizes glucose to 2-ketogluconate in the periplasm, which can be released to the medium, the finding of 2.6 mM 2-ketogluconate expelled into the medium after 2 h of growth is strong evidence that the cells were oxidizing glucose from the LB but were not catabolizing it in the cytoplasm. By mid exponential phase (3 h of growth), the concentration of glucose polysaccharides was reduced to almost half of the initial, and further fell during the late exponential phase (Fig. 1C). This was not paralleled by an accumulation of 2-ketogluconate in the medium, which suggests that glucose and 2-ketogluconate were now being metabolized in the cytoplasm.

Amino acids were used in a sequential and hierarchical manner. Early exponential growth was characterized by the significant consumption of glutamate/glutamine, lysine, leucine, alanine, aspartate/asparagine, valine, isoleucine, proline, phenylalanine, threonine and serine, the consumption rate being highest for glutamate/glutamine (Supporting Information Table S1). The pattern changed during mid exponential growth when the consumption of many of these amino acids decreased significantly (glutamate/glutamine, leucine, aspartate/asparagine, valine, proline and threonine), or even ceased completely (lysine, alanine, isoleucine and phenylalanine). During this period; however, the consumption of serine and methionine increased. The late exponential phase showed a different pattern again: the consumption of glutamate/glutamine, arginine, leucine, alanine and isoleucine increased once more, and low consumptions of glycine and histidine were detected. This is in general agreement with earlier work showing that, during the first 2–3 h of growth in LB, *P. putida* consumes asparagine, aspartate, serine, proline and glutamate/glutamine, while the assimilation of alanine, arginine, glycine, leucine and isoleucine is delayed until after 4–6 h of culture, the remaining amino acids being used only when cells are in the stationary phase (La Rosa *et al.,* 2016). However, these sets of results should be compared with care, since this earlier work focused on the consumption of free amino acids only; in the present work, the consumption of both free amino acids and those present as peptides was measured. The amino acids consumed most strongly throughout the growth period examined were glutamate/glutamine, aspartate/asparagine, arginine and serine (Supporting Information Table S1).

Finally, the ammonium concentration in the medium slowly increased over growth, a likely consequence of the assimilation of amino acids. The pH of the medium showed a small increase during the first 2 h of growth and raised from 6.8 to 7.6 during the mid to late exponential phase (Supporting Information Table S1). This is consistent with the preferential use of sugars and organic acids during the first 3 h of growth, and a switch to amino acids thereafter.

Modelling the metabolic fluxes at different moments of exponential growth

To understand, in terms of flux distribution, the mechanistic meaning of the nutrient consumption profiles observed experimentally during the early, mid and late exponential phases of growth, we took the advantage of the latest genome-scale metabolic model available for *P. putida* KT2440, named *i*JN1411. This model accounts for 2826 metabolic and transport reactions and 1411 genes and offers a solid representation of *P. putida* metabolism (Nogales *et al.,* 2008, 2017). Condition-specific models corresponding to the metabolic status of the early, mid and late exponential phases were constructed using the experimentally acquired data for the consumption or secretion of metabolites indicated in Supporting Information Table S1. The solution space for each model was examined by flux-balance analysis by maximizing growth rate as the objective function. The subsequent comparison

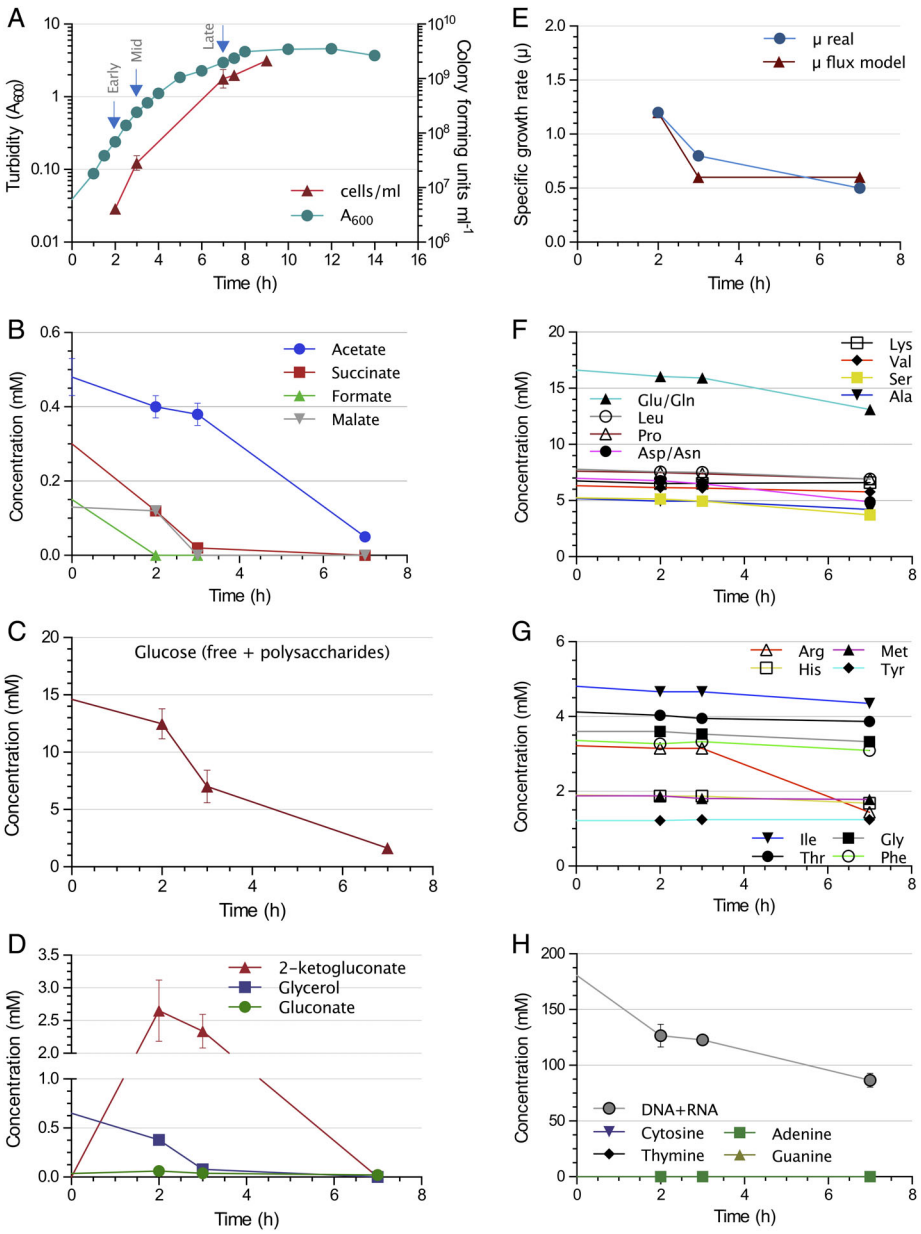

Fig. 1. Growth of *P. putida* KT2440 in LB and consumption of different compounds.
A. Increase in turbidity (A_{600}) and in colony forming units (cells/ml) during growth in LB. Consumption of organic acids (B), sugars (glucose monomers and polymers) (C), amino acids (F, G) and (poly) nucleotides (H) during growth.
D. Release of 2-ketogluconate and gluconate to the medium and consumption of glycerol during growth.
E. Growth rate at each time point relative to the previous point (or to the inoculated cells in the case of the first time point); data derived either from the experimentally determined increase in biomass (μ real), or from the increase predicted by the flux model (μ flux model). Error bars indicate the standard deviation of three independent assays. The scale of the time axis is not the same in all panels.

of fluxes distribution between the different condition-specific models allowed the identification of the metabolic shifts that occur throughout the three *P. putida* growth periods analysed. The growth rates (μ) predicted by the model for each time point fitted well with those experimentally determined, with a Kendall's rank correlation coefficient of 0.90 (Fig. 1E). Since any deviation between the *in vivo* and *in silico* growth rates indicates the experimental data to be incomplete, these results strongly support the correct capture of the uptake rates for the nutrients being assimilated *in vivo* and bear witness to the accuracy of the condition-specific models constructed.

The proteome of cells collected at the early, mid and late exponential phase were analysed and compared to each other to confirm that the changes in the predicted metabolic fluxes agreed with the increase or reduction in the proteins involved in the corresponding metabolic pathways. More than 1782 proteins were detected, of which between 10.6% and 31.2% changed in abundance during the different phases (Fig. 3A). A visual representation of the changes observed (Fig. 3B) shows that the proteome undergoes substantial change during growth. Of note, when comparing the mid exponential phase with the early phase, most of the differentially expressed proteins were down-regulated. The opposite was observed during the late exponential phase, since most of the differentially expressed proteins relative to the previous phases were up-regulated. The configuration of the

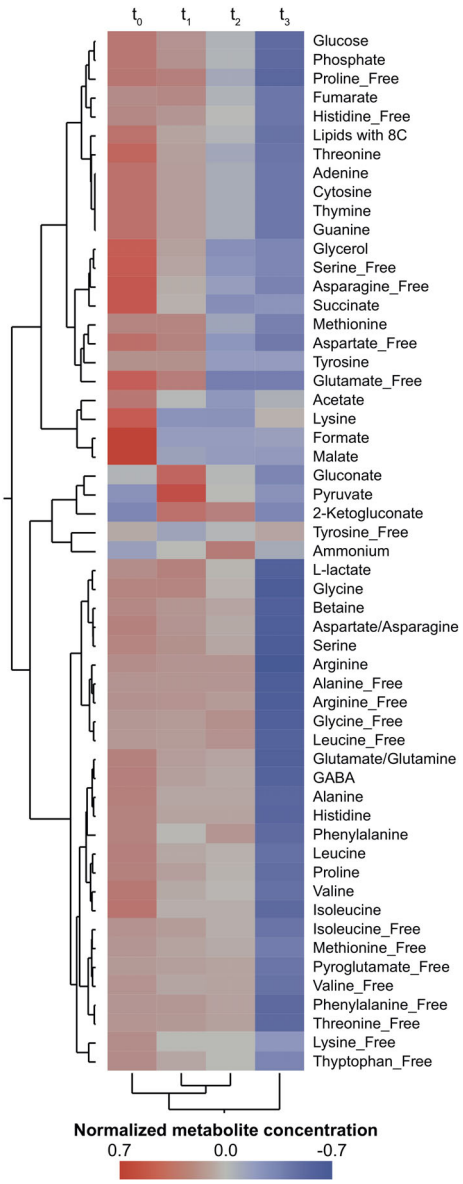

Fig. 2. Hierarchical clustering of the exo-metabolomic profiles of *P. putida*. The normalized concentrations (range scaling) of each metabolite identified in the noninoculated medium (t0), or in medium samples collected at the early (t1), mid (t2) and late (t3) exponential phases of growth (data derived from Supporting Information Table S1), were clustered according to Euclidean distances using the Ward clustering algorithm (Ward Jr, 1963) and employing JMP software v.13.2. The highest normalized concentration for each compound is indicated in red colour, while the lowest concentration is in blue.

metabolic fluxes at each growth phase deduced from these complementary approaches is described below.

Configuration of metabolism during the early exponential phase

Feeding the *i*JN1411 metabolic model with the nutrients exchange rates experimentally determined during the early exponential phase, as indicated in Supporting Information Table S1, allowed an accurate prediction of the metabolic fluxes driving growth during this period. Metabolism at this stage was characterized by the strong oxidation of glucose polymers such as glycogen, maltodextrin (obtained by the partial hydrolysis of glycogen), or β-glucans. *P. putida* is not able to use glucose polymers or mannose polymers when provided as the sole carbon source (Dvorak and de Lorenzo, 2018). In fact, the present work confirmed that strain KT2440 cannot grow on starch, cellobiose, maltodextrin, or yeast mannan alone. However, adding a limiting amount of glutamate (5 mM) allowed for robust growth in the presence of starch, cellobiose or maltodextrin (but not mannan), growth that was much faster than that achieved with glutamate alone (Supporting Information Fig. S2). This suggests that strain KT2440 can somehow profit from these glucose polymers if supplemented with an additional carbon and energy source. However, it would not profit from mannose polysaccharides.

Glucose (free monomers plus that forming polymers) was present in the fresh LB at 14.62 mM (Supporting Information Table S1). During the early exponential growth, the model-based predictions evidenced that glucose was not transported to the cytoplasm but was rather oxidized in the periplasm to 2-ketogluconate via gluconate and subsequently excreted to the medium together with a small quantity of gluconate (Fig. 4 and Supporting Information Fig. S3A). The oxidation of glucose to 2-ketogluconate, which is coupled to the reduction of the membrane quinones, would render large amounts of reduced quinones to feed the respiratory chain. In support of this, the proteins involved in the uptake and initial oxidation of glucose in the periplasm were detected in the proteome of cells during the early exponential phase of growth, and the concentrations of 2-ketogluconate and gluconate in the growth medium increased after 2 h of growth, confirming that the expulsion of these compounds was indeed taking place (Supporting Information Table S1 and Fig. 1D).

The tricarboxylic acids cycle (TCA) in this early phase of growth should rely on the influx of organic acids that are intermediates of this cycle, for example, citrate, malate and succinate, plus amino acids that are ultimately converted into cycle intermediates, that is, arginine (renders succinate), glutamate (renders α-ketoglutarate) or ornithine (renders fumarate) (Figs. 4 and Fig. 5 and Supporting Information Fig. S3). The model predicted that, during this early phase, the TCA cycle ought to operate under an anaplerotic configuration driven by the glyoxylate shunt exclusively, the α-ketoglutarate dehydrogenase complex being inactive (Fig. 4 and Supporting Information Fig. S3). As a consequence, a large flux from TCA to G3P was predicted following anaplerotic pathways via oxaloacetate. Ultimately, the G3P produced would be funnelled to glucose 6-phosphate (G6P) via gluconeogenesis. Consistently, most of the enzymes required for these reactions

A

Growth phases compared	Total proteins compared	Differentially expressed	Upregulated proteins	Downregulated proteins
Mid / early	1785	189	13	176
Late / early	1782	446	360	86
Late / mid	1792	557	521	26

B

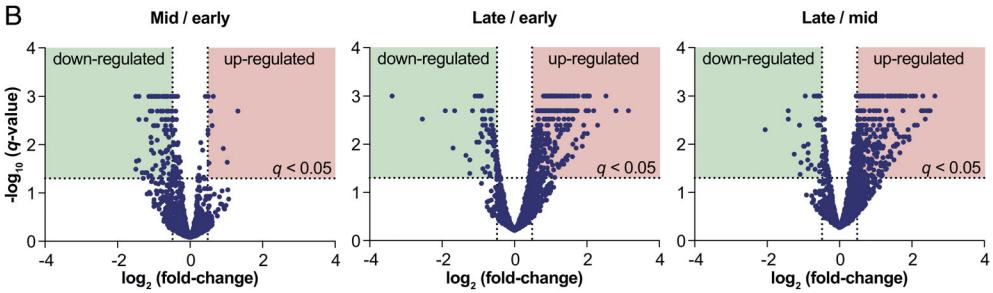

Fig. 3. Comparison of the proteome of cells collected at early, mid and late exponential growth.
A. Number of proteins detected and compared under each condition, and those differentially expressed (q-value<0.05, fold-change >1.4, as recommended (Koul et al., 2014)).
B. Volcano plots of the proteins showing increased or decreased abundance during early, mid and late exponential growth. Differentially expressed proteins are listed in Supporting Information Table S2.

were detected in the proteome. These metabolite fluxes towards G6P indicate cells to be operating in a gluconeogenic configuration, which is consistent with the idea that all glucose consumed is oxidized in the periplasm but does not enter the cell during early exponential growth. The model further predicted that the G6P generated would be used to synthesize polysaccharides.

Under this scenario, model-based predictions suggested a potential metabolic overflow towards pyruvate. In fact, a large flux from oxaloacetate to pyruvate was predicted via the action of the Prp proteins belonging to methyl-citrate cycle. In addition, pyruvate would also be produced by the transamination of alanine. Around two thirds of this pyruvate would be transformed into acetyl-CoA, and the rest released to the medium either directly or after conversion to lactate (Supporting Information Fig. S3A). In support of this flux configuration, the Prp proteins were detected in the proteome of cells in the early growth phase (Supporting Information Fig. S3A), while the secretion of pyruvate and lactate was experimentally confirmed (Supporting Information Table S1).

The model predicted as well as an intense flux through amino acid metabolism pathways, which were responsible for providing nitrogenous building blocks for protein and nucleotide biosynthesis. This scenario was largely supported by the anaplerotic configuration of TCA described above. For instance, glutamate/glutamine showed the highest rate of uptake of all the amino acids analysed during the early exponential growth (Supporting Information Table S1). The flux model predicted that glutamine would be transformed into glutamate in the periplasm by the glutaminase-asparaginase (AnsB), which would be internalized and used as a source of α-ketoglutarate, glutamine and ornithine (Fig. 5 and Supporting Information Fig. S3B). Glutamine would be used in the biosynthesis of asparagine, histidine and nucleotides, while ornithine would be instrumental as an additional source of arginine. Proline would also be transported from the external medium and transformed into glutamate, although the uptake rates would be about a quarter that of glutamate.

The predicted fluxes highlighted an important role for aspartate and asparagine in nitrogen/carbon metabolism during early exponential growth. The uptake rates measured for these amino acids during this phase were a third that of glutamate but still important (Supporting Information Table S1 and Fig. S3B). The model predicted that asparagine would be transformed into aspartate in the periplasm by the AnsB enzyme, and therefore enter the cell as aspartate, which participates in the metabolism of methionine, arginine, fumarate, oxaloacetate and nucleotides. Leucine and lysine were consumed at detectable rates. Alanine, isoleucine and valine were predicted to be catabolized to pyruvate and succinate. Lysine, instead, would be transformed into glutarate, and then released to the medium. The uptake rates for serine, threonine, phenylalanine, arginine and proline were about an eighth to a sixth that of glutamate (Supporting Information Table S1). Supporting Information Figure S3B shows the fate of each amino acid. Overall, the model predicted that ammonium generated from the metabolism of these amino acids would be used in part to form carbamate (involved in the generation of nucleotides and arginine), the rest being released into the medium. This expulsion was experimentally confirmed (Supporting Information Table S1). The carbon flux prediction also highlighted the use of betaine and threonine as the sources of glycine during early exponential growth. This glycine would be further degraded to render ammonium, CO_2 and reducing equivalents through the glycine-cleavage systems (Supporting Information Fig. S3B).

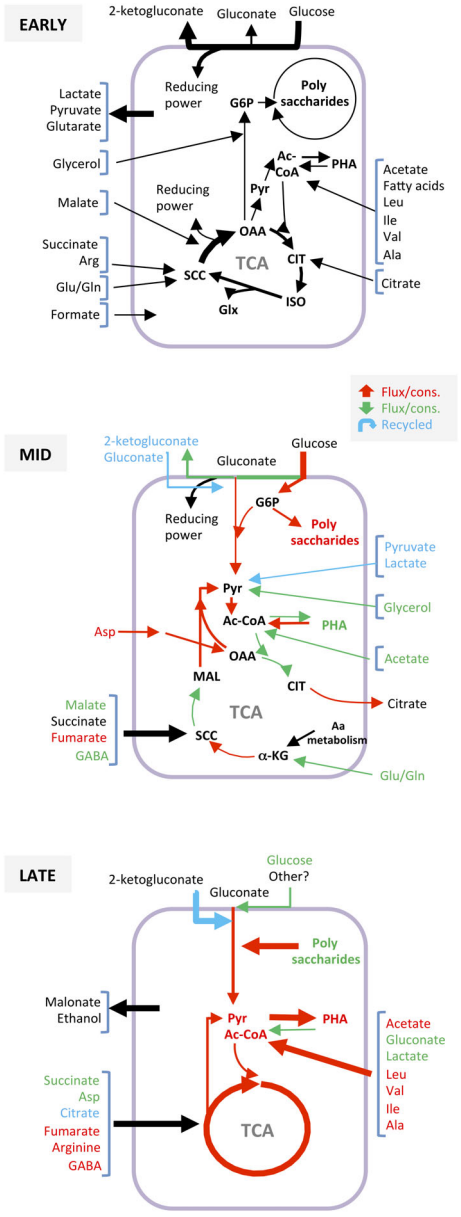

Fig. 4. Configuration of the metabolite fluxes related to central carbon metabolism during early, mid and late exponential growth. Summary of the metabolite fluxes as predicted by the *i*JN1411 metabolic model constrained by the consumption data as indicated in Supporting Information Table S1. The fluxes corresponding to the early exponential phase are indicated in black. Fluxes that change at later times of growth are indicated in red (increased flux) or green (decreased flux). Compounds that are released to the medium and later recycled are indicated in blue. A more detailed distribution of the fluxes is given in Supporting Information Figs S3A (early exponential phase), S4 (mid exponential phase) and S6 (late exponential phase). TCA, tricarboxylic acids cycle; G6P, glucose-6-phosphate; Ac-CoA, acetyl-CoA; PHA, polyhydroxyalkanoates; OAA, oxaloacetate; SUC, succinate; ISO, isocitrate, MAL, malate; CIT, citrate, Pyr, pyruvate, α-KG, α-ketoglutarate.

Therefore, glycine was predicted to be used as an efficient energy source but not as a carbon source (Supporting Information Fig. S3B).

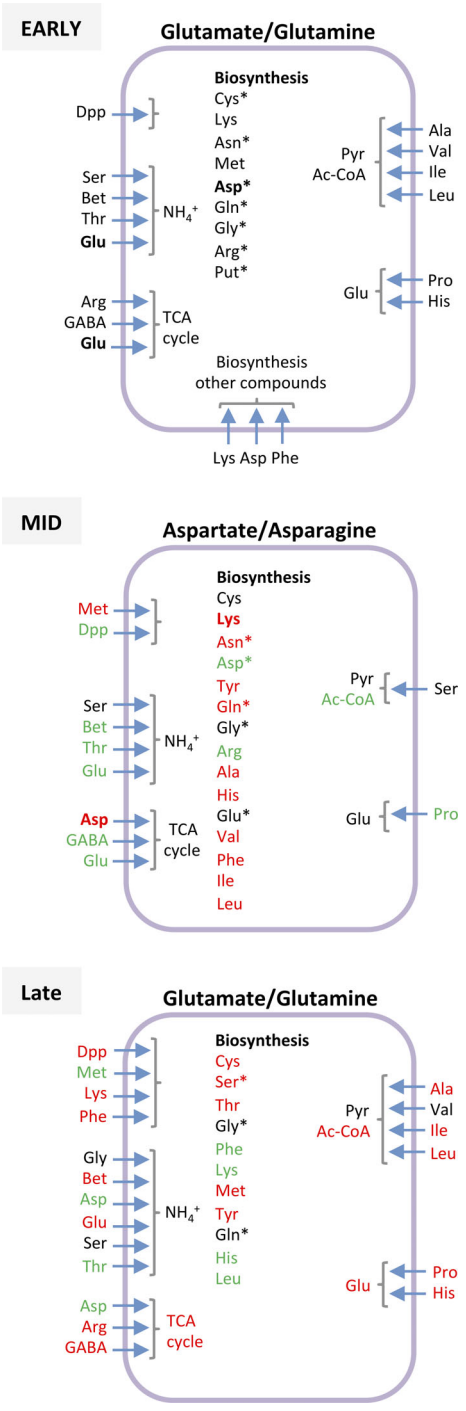

Fig. 5. Metabolism of amino acids during early, mid and late exponential growth. Summary of the fate of the amino acids used as predicted by the *i*JN1411 metabolic model constrained by the consumption data as indicated in Supporting Information Table S1. Those used during the early exponential phase are indicated in black. Amino acids for which consumption increased (red) or decreased (green) relative to early exponential growth are highlighted. Those that, after their uptake, are biodegraded within cells are indicated with an asterisk. A more detailed distribution of the fluxes is given in Supporting Information Figs S3B (early exponential phase), S5 (mid exponential phase) and S7 (late exponential phase).

Overall, nutrients exchange, proteomic analysis and flux prediction during early exponential growth phase suggested that sugars were used as the main energy source via periplasmic oxidation, relegating TCA to a simple anaplerotic assistance. On the contrary, the intense metabolism of amino acids observed was responsible for providing nitrogenous building blocks rather than energy.

Finally, the model-based predictions also suggested that, during early exponential growth, polyhydroxyalkanoates (PHAs) would be both synthesized and degraded, the total flux being positive for synthesis. This would require the use of various compounds from the medium catabolized via acetyl-CoA and known to be good precursors of PHA such as acetate, fatty acids, and branched chain amino acids (Fig. 4 and Supporting Information Fig. S3A). This agrees with previous reports showing that, in strain KT2440, PHAs are constantly synthesized and degraded even under balanced carbon/nitrogen conditions in order to adapt the carbon flow and reducing power to the demand for cellular intermediates (Escapa *et al.,* 2012). The PhaF and PhaI proteins, which are associated to the PHA granules, were detected in the cell's proteome (Supporting Information Table S2).

Configuration of metabolism during mid exponential phase

The consumption of sugars, which was strong during the early exponential growth, continued during the mid exponential phase (Supporting Information Table S1). However, while in the initial phase the model predicted that all glucose would be oxidized in the periplasm and the resulting compounds (gluconate and 2-ketogluconate) excreted into the medium, during the mid exponential phase only a small fraction of glucose would be oxidized in the periplasm to form gluconate, and most glucose molecules would enter the cell and be converted into G6P. A small part of this G6P would be funnelled to the glycolytic Entner-Doudoroff pathway, while the rest would be directed to the synthesis of glucose-polysaccharides (cellulose, alginate or glycogen) (Fig. 4 and Supporting Information Fig. S4). In agreement with these predictions, the expressions of the 1,4-α-glucan branching enzyme GlgB and the glycogen phosphorylase GlgP, which are involved in glycogen metabolism, were lower at the mid exponential phase than during the initial phase (Supporting Information Table S2). The expression of the glycogen synthase GlgE, involved in the elongation of α-(1,4)-glucans, did not vary during these two phases of growth. This suggests that cells were synthesizing glycogen during both, but since degradation decreased during the mid exponential phase, a net accumulation of glycogen occurred. The enzymes involved in cellulose biosynthesis were also detected in the proteome, although their expression did not change. Those involved in alginate biosynthesis were not detected.

The fluxes through the TCA were predicted to suffer several changes during mid exponential growth. In fact, the TCA configuration would turn from an anaplerotic to an oxidative mode. This change was sustained by an inhibition of the glyoxylate shunt and the activation of the oxidative step catalysed by α-ketoglutarate dehydrogenase. However, the TCA oxidative mode was far from complete as the other two key steps of the oxidative branch, that is, isocitrate dehydrogenase and aconitase, were predicted to be inactive. As a result, the transformation of citrate into isocitrate would diminish and the citrate accumulated would be released to the medium (Fig. 4; compare Supporting Information Figs. S3A and S4A). Consistently, the metabolism of amino acids (see below), but not the isocitrate dehydrogenase, was predicted to be the main source of α-ketoglutarate, while the flux through the TCA reductive branch was significantly lower than in early growth phase due the absence of glyoxylate shunt as source of succinate. In support of this flux configuration, proteomic analyses indicated that the abundance of the glyoxylate-shunt enzymes AceA and GlcB, as well as that of some isoforms of aconitase (AcnA), isocitrate dehydrogenase (Icd) and fumarase (FumC-II), decreased significantly during mid exponential phase (Supporting Information Fig. S4B and Table S2). The abundance of the remaining isoforms of these same enzymes (AcnB, Idh, FumA, FumC-I) was similar during the early and mid exponential phases of growth.

Another modification of the TCA cycle was a change in the fate of malate. Rather than follow the TCA cycle to render oxaloacetate via malate dehydrogenase, as it occurred in the early exponential phase, during the mid exponential phase the model predicted the activation of the pyruvate shunt driven by the malic enzyme (Fig. 4 and Supporting Information Fig. S4A). This would result in an increase in the NADPH levels that could be used to fight the reactive oxygen species (ROS) derived from the increase in oxidative metabolism predicted at this stage.

Regarding amino acids metabolism, it is worth noting that the consumption of lysine, alanine, valine, isoleucine, leucine, histidine and arginine decreased strongly when the cells entered the mid exponential phase, while phenylalanine appeared to be released to the medium (Supporting Information Table S1). The cells now consumed glutamate, aspartate/asparagine, threonine, serine, methionine and proline (Supporting Information Table S1; Figs. 1F and Fig. 5, Supporting Information Fig. S5A). Accordingly, the flux model predicted that *P. putida* KT2440 metabolism would suffer reorganization in order to synthesize the amino acids now in shorter supply. Proteomic analyses were in general agreement with these predictions and showed that entry into the mid exponential growth was paralleled by a

reduction in the abundance of the enzymes corresponding to many—though not all—pathways for the degradation of amino acids (Supporting Information Fig. S5B, green arrows; Supporting Information Table S2). In contrast, a significant increase in the abundance of proteins involved in the methionine and aspartate transport was observed, in agreement with the detected increase in the use of these amino acids. The absence of changes in the abundance of the enzymes involved in the biosynthesis of amino acids, and the reduction in those involved in their degradation, suggests a net flux balance directed towards the biosynthesis of amino acids, just as predicted by the condition-specific model. In agreement with this active anabolism, with the depletion of several metabolites in this stage such as fatty acids, and with the requirement of additional carbon skeletons, model-based predictions suggested cells cease to produce PHAs, with the existing polymer reserves being degraded (Fig. 4 and Supporting Information Fig. S4A). Proteomic analyses (Supporting Information Table S2) agreed with this prediction since a reduction was detected in the abundance of the PhaF and PhaI proteins associated to the PHA granules. In the same line, the secretion of lactate and pyruvate would cease; in fact, they were recovered from the medium and catabolized (Fig. 4 and Supporting Information Fig. S4A; Supporting Information Table S1).

Taken together, the analysis of metabolic fluxes in the mid exponential phase suggested that sugar oxidation in the periplasm was partially replaced by the TCA as the main source of energy. In addition, the progressive depletion of preferred metabolites likely forced cells to adopt a more efficient metabolism of glucose, starting its complete mineralization. Finally, it seems that *P. putida* displayed a metabolite recovery program in this stage to supply the higher demand of carbons skeleton required for anabolism.

Configuration of metabolism during the late exponential phase

Seven hours after inoculation, the increase in biomass and in total cell numbers indicated that cells were still actively growing at a rate similar to that observed during the mid exponential phase, although exponential growth was reaching its end (Fig. 1A and E). Most of the changes observed during the transition from the early to the mid exponential phases were now reverted. The use of glucose decreased substantially during the late exponential phase (Supporting Information Table S1 and Fig. 1C). The model predicted that all glucose entering the cell would be transformed into gluconate in the periplasm by the glucose dehydrogenase Gcd, with all gluconate entering the cytoplasm (Fig. 4 and Supporting Information Fig. S6A). About 90% of this gluconate would be transformed into pyruvate via the Entner–Doudoroff pathway, which would be used to synthesize acetyl-CoA. The remaining 10% would be diverted to the pentose phosphate pathway to form ribulose-5-phosphate, G3P and fructose-6-phosphate. The flux model predicted that the cells would reduce or cease the synthesis of intracellular glucose polymers (Fig. 4). In agreement, the abundance of the glycogen synthase GlgE was found to be reduced, while those of GlgB (1,4-α-glucan branching enzyme) and GlgP (α-1,4 glucan phosphorylase) increased (Supporting Information Table S2). This suggests that, when entering the late exponential phase, cells degrade the polysaccharides accumulated in the previous phase to obtain glucose.

In addition, the incipient oxidative mode of TCA adopted during the mid exponential phase became more evident during this late growth phase and the flux model predicted that the cycle would be fully activated (Fig. 4). In agreement with this prediction, many of the cycle enzymes became more abundant during the late exponential phase (Supporting Information Fig. S6B, red arrows, and Supporting Information Table S2). The increase was observed for all isoforms of the enzymes affected with the exception of succinyl-CoA synthetase (SucC and SucD) and succinate dehydrogenase (SdhABCD), which were already abundant during the previous growth phase, and the enzymes that oxidize malate (Mdh remained constant, Mqo-1 increased, and Mqo-2 decreased).

The flux model predicted an increase in the rate of degradation of fatty acids at this point. In agreement with this, the abundance of several enzymes responsible for the β-oxidation of fatty acids (FadA, FadBA, FadB, the enoyl-CoA hydratase PP_1845, FadE) was found to be increased relative to the previous phase (Supporting Information Fig. S6B and Table S2). The abundance of proteins related to acetate generation (AcsA) and PHA metabolism (BktB, Hbd, PhaC1 and PhaF) also increased (Supporting Information Fig. S6B). All this led to the pool of acetyl-CoA becoming larger and an increase in the synthesis of PHAs, as predicted by the flux model. In agreement with this idea, the abundance of the enzymes involved in the glyoxylate shunt also increased in order to metabolize the acetyl-CoA produced.

The metabolism of amino acids also changed when the cells reached the late exponential phase. Proteomic analyses and model predictions suggested the cells to now grow at the expense of amino acids. The uptake of arginine, alanine, leucine, isoleucine, glutamate/glutamine and histidine increased. The transport of glutamate remained active, allowing it to serve as a donor of amine groups for the biosynthesis of other amino acids. Importantly, proteins annotated as oligopeptide transporters increased in abundance, which might allow cells to use serine or proline, the free forms of which would likely have been exhausted during the earlier phase of growth (La Rosa *et al.,* 2016). Other transporters were activated during late

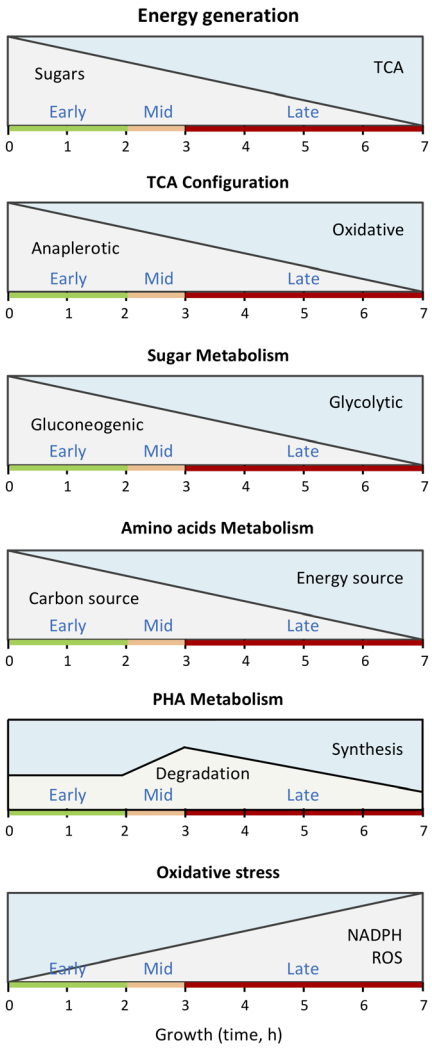

Fig. 6. Modifications in the configuration of *P. putida* KT2440 metabolism during the early, mid and late phases of its exponential growth in LB. The changes observed in the strategies to obtain energy (reducing power), the TCA configuration, the metabolism of sugars, amino acids and PHAs, as well as in the generation of oxidative stress, are indicated. The representation is merely schematic and by no means quantitative.

exponential growth, such as those for the polyamine putrescine and γ-aminobutyric acid (GABA). The direct determination of GABA showed that it was indeed present in the initial LB at low concentration but had been largely consumed by this point in growth (Supporting Information Table S1). In contrast, the uptake rates for methionine, aspartate and threonine were experimentally observed to decrease (Supporting Information Table S1 and Fig. 5), as was the abundance of proteins involved in their transport (Supporting Information Fig. S7B). This intense catabolism of amino acids is consistent with the fully oxidative mode of TCA as main source of energy.

Finally, it is worth noting that the metabolism of glutathione was activated during late exponential growth. An increase was detected in the abundance of the enzymes involved in its biosynthesis (GshB glutathione synthetase) and degradation (Ggt γ-glutamyltranspeptidase and PepN aminopeptidase) (Supporting Information Fig. S7B and Table S2). This tripeptide reduces oxidized proteins. The abundance of the glutathione reductase Gor, which regenerates oxidized glutathione, also increased, as did that of several enzymes involved in the detoxification of ROS, such as the catalases KatA and KatG, the alkylhydroperoxide reductase AhpC, and the peroxidase Tpx. All this suggests that the cells were exposed to oxidative stress during this late phase of growth. The use of the 2,3,5-triphenyl-2H-tetrazolium chloride (TTC) reduction assay showed that the redox state of the cells was low during the early and mid exponential phases but increased significantly during the late exponential phase (Supporting Information Table S1). This indicates that during the latter phase, the concentration of ROS increases, which fully agrees with the TCA fully operating in an oxidative mode.

Discussion

When preferred compounds are exhausted early during growth in a complete medium such as LB, cells need to adapt their metabolism towards the less preferred compounds that remain. By visualizing the metabolic fluxes at three moments during exponential growth in LB, the present work provides greater insight in this issue by reconstructing the dynamic carbon flux readjustment driving this behaviour. The results, which are summarized in Fig. 6, show for the first time how, when using this medium, *P. putida* completely changes the configuration of its central and peripheral metabolism during exponential growth in response to changing nutrient availability. During growth from the early to the late exponential phase, we monitored a gradual change in (i) the mode of energy generation; (ii) the TCA configuration, which changed from anaplerotic to oxidative; (iii) the metabolism of sugars, which changed from gluconeogenic to glycolytic; (iv) the metabolism of amino acids, which were first used as carbon source and later on as energy source, and (v) the carbon storage metabolism. This gradual change was paralleled by a lineal increase in ROS generation, which was retaliated by an increase in NADPH generation. It seems plausible that *P. putida* avoids unnecessary cytoplasmic anabolism and oxidative metabolism, while minimizing the production of ROS under nutritionally rich conditions. Depletion of preferred nutrients forced *P. putida* to adopt a more efficient oxidative metabolism, which was balanced with a higher NADPH production to minimize potential deleterious effects due the expected increase in ROS.

The control of metabolic fluxes in response to the concentration of key metabolites is a complex and poorly known phenomenon that is of vital importance to coordinate

microbial metabolism (Chubukov *et al.,* 2014). Cells began growth using organic acids such as acetate and different TCA intermediates (citrate, malate and succinate), and a selected set of amino acids (mostly glutamate/glutamine), as their carbon sources. Sugars (glucose monomers and apparently glucose polymers derived from yeast extract) were also consumed during this early stage, but the proteomic data collected, the flux model, and the detected secretion of 2-ketogluconate, all indicate that these sugars were not used as a carbon source but as a supply of electrons to feed the electron transport chain, that is, they were used as energy source. The oxidized sugar products were mostly released into the medium. Glucose polymers were present in substantial concentrations. It should be stressed that different sources of yeast extract can include different amounts of sugars, which might influence the metabolic configuration of cells.

It is still not clear how cells managed to use glucose polysaccharides. Although *P. putida* KT2440 could not grow on starch, cellobiose or maltodextrin alone, robust growth occurred if a limiting amount of glutamate was provided as well (Supporting Information Fig. S2). This suggests that *P. putida* can in fact profit from these sugar polymers. The genome of strain KT2440 encodes some enzymes that might be instrumental in depolymerising glucose polymers. These include PP_1403 (BglX), a periplasmic glucohydrolase that catalyses the hydrolysis of glycosidic bonds in β-D-glucans with the release of glucose, and the product of PP_1126, which codes for a periplasmic glycoside hydrolase. Both these enzymes were detected in the cell proteome, although their abundance seemed to change little throughout growth. Cells might secrete other glucanases that escaped the present proteomic analyses.

During the early growth phase, the TCA cycle seemed to operate solely via the glyoxylate shunt, a configuration characteristic of situations in which cells grow at the expense of 2- or 3-carbon organic acids, or fatty acids (Fig. 4). This means that isocitrate dehydrogenase and α-ketoglutarate dehydrogenase, which are important providers of NADH, were not active, and most energy (reducing power) was provided by the oxidation of glucose in the periplasmic space, and by oxidation of the glycine produced from threonine and betaine. In *Pseudomonas aeruginosa*, flux distribution between the TCA cycle and the glyoxylate shunt is coordinated through the reciprocal regulation of isocitrate dehydrogenase and isocitrate lyase; low concentrations of oxaloacetate and pyruvate inhibit isocitrate dehydrogenase and activate isocitrate lyase, favouring the glyoxylate shunt and reducing the flow through the TCA (Crousilles *et al.,* 2018). Our results are consistent with oxaloacetate and pyruvate being in short supply during the early growth phase and suggest that a flux from oxaloacetate towards glucose-6P occurred, the cells being in a gluconeogenic configuration.

This metabolic configuration changed as the cells entered the mid exponential phase, with the contribution of organic acids and several amino acids decreasing substantially. Unsurprisingly, the cells turned to glucose to sustain their growth and some glucose and gluconate molecules now entered the cell and were directed either towards the TCA cycle or to the synthesis of polysaccharides. The TCA cycle was also fed via the increased uptake of aspartate and the recycling of compounds excreted in the previous phase, such as pyruvate and 2-ketogluconate. This sudden funnelling of metabolites towards TCA could not be processed properly and a bottleneck appeared resulting in the secretion of citrate. A few hours later, when the cells entered into the late exponential phase of growth, this picture changed again substantially. The use of sugars as a carbon source continued; this was reinforced by the depolymerisation of the polysaccharides accumulated intracellularly in the previous phases. Several amino acids, most notably arginine, were used as a source of TCA intermediates, and the citrate extruded in the previous phase was recovered and processed in the TCA cycle, which now started to function actively in a fully cyclical manner, that is, in its fully oxidative mode, increasing the supply of NADH. This was paralleled by an increase in the production of ROS and in the elements devoted to fight oxidative stress (glutation, catalases, etc). The cells used different amino acids in each growth phase, the bias between amino acid synthesis and degradation shifting towards synthesis during the mid exponential phase and returning towards degradation in the late exponential phase.

All the data collected are consistent with the sequential and hierarchical use of the compounds present in LB, and a progressive rearrangement of the cells' metabolism so that the way of obtaining energy and carbon building blocks evolved and adapted to the continuously changing conditions. All these changes occurred without any noticeable interruption in cell growth, although perhaps cells experienced multiple, shifting limitations, as suggested earlier (Wittgens *et al.,* 2011). This might be the result of gene expression being highly optimized, but also of the fact that, despite the hierarchical assimilation of the compounds present, several were used simultaneously at each time point, the exhaustion of one being compensated by the assimilation of alternatives. The overall picture, therefore, is that of a very flexible and well-coordinated metabolism that allows adaptation to the prevailing conditions, while maintaining vigorous growth. It is worth stressing that, despite the strong use of sugars through growth, glucose transport and assimilation is known to be under catabolite repression, a process controlled by the Hfq/Crc proteins. Inactivating the gene coding for Crc increased the glucose assimilation rate and the expression of the genes involved in the transport and assimilation of glucose (del Castillo and Ramos, 2007;Moreno *et al.,* 2009 ; La Rosa *et al.,* 2016).

The results presented here show that this repression did not impede the use of glucose (or glucose polymers) as an energy source at the start of growth, although neither glucose nor glucose oxidation products appeared to be used as a carbon source until the second period of the exponential growth. This indicates that the regulation of glucose assimilation is complex.

Inactivation of the gene coding for the Crc protein is known to cause an 8%–10% reduction in the growth rate of strain KT2440 in LB; its metabolism is destabilized and cell fitness reduced, allowing wild type cells to rapidly out-compete the mutant strain (Moreno *et al.,* 2009; La Rosa *et al.,* 2016). This shows that catabolite repression is involved in the optimisation of metabolism, which helps explain the success of *P. putida* as an opportunistic and cosmopolitan bacterium. A detailed knowledge of the metabolic fluxes that operate under different growth conditions is essential, if we are to understand how cells function, and if we are to use their metabolism for desired ends. The present results are a step in this direction.

Experimental procedures

Bacterial strains and culture media

P. putida KT2440 (Franklin *et al.,* 1981) was cultured at 30 °C in LB (10 g/l tryptone, 5 g/l yeast extract, 10 g/l NaCl). Tryptone and Yeast Extract were obtained from Conda (Spain). The ability of this bacterial strain to use polysaccharides as the carbon source was determined in M9 minimal salts medium (Sambrook and Russell, 2001) supplemented with trace elements (Bauchop and Eldsen, 1960); its final composition was 42.4 mM Na_2HPO_4, 22 mM KH_2PO_4, 8.6 mM NaCl, 18.7 mM NH_4Cl, 25 μM $CaCO_3$, 1.2 μM $CoSO_4$, 1.3 μM $CuSO_4$, 42.7 μM $FeSO_4$, 0.4 μM H_3BO_3, 776 μM HCl, 333 μM MgO, 38.1 μM $MnSO_4$, 6.25 μM $ZnSO_4$. The polysaccharides tested were potato starch, cellobiose, maltodextrin and mannan (from *S. cerevisae*). These were added at 0.25% (w/v) in the presence or absence of 3 mM glucose or 5 mM glutamate.

Determination of chemical compounds in LB during P. putida *growth*

Twenty millilitres of fresh LB were inoculated with overnight cultures of the microorganism at a turbidity (A_{600}) of 0.05. The cultures were incubated at 30 °C to an A_{600} of 0.2 (early exponential growth), 0.6 (mid exponential growth) or 2 (late exponential growth). At these time points they were centrifuged at 7500 × rpm for 10 min and the supernatants obtained filtered through 0.22 μm pore filters (Millipore-Merck) to eliminate cells. Then, they were frozen at −80 °C until analysis. The content of sugars, organic acids and amino acids in these samples was analysed using previously described methods. To determine the total amount of glucose, glucose polysaccharides in the samples were hydrolysed by treatment with 2 M trifluoroacetic acid at 120 °C for 1 h. Glucose was then detected by HPLC using a 920LC Agilent apparatus equipped with a PL-EDS 2100 Ice detector and an Asahipak NH_2-50 E column (Shodex). The mobile phase was an acetonitrile/water gradient as follows: t = 0, 77%; t = 10, 77%; t = 17, 65%; t = 20, 65%; t = 20.1, 77%; t = 25, 77% (t in min, % refers to acetonitrile concentration); the flow rate was 1.2 ml/min. Three independent assays were performed.

The content of 2-ketogluconate was determined as previously described (Lanning and Cohen, 1951). In brief, 1 ml of 2.5% (w/v, in water) *o*-phenylenediamine dihydrochloride was mixed with 2 ml of LB or filtered culture supernatants. After heating in boiling water for 30 min, the absorbance of the reaction mixture was measured at 330 nm. A standard curve was prepared using different concentrations of 2-ketogluconate. Three independent assays were performed.

Gluconate, lactate and fatty acid concentrations were determined using the D-gluconic acid/D-glucono-δ-lactone assay kit (Megazyme), the Lactate Assay Kit (Sigma-Aldrich), and the Free Fatty Acid Quantification Kit (Sigma-Aldrich, St. Louis, Missouri), respectively. Polynucleotide quantification was performed using the DNA Quantification Kit (Sigma-Aldrich) and the Quant-iT Oligreen ssDNA Kit (Thermo Fisher Scientific). The consumption of individual nucleotides was estimated on the basis of the G + C content of *S. cerevisae* (38%). The concentrations of α-ketoglutarate, citrate, GABA, isocitrate and malate were determined by HPLC/MS using a 1200 l Varian device fitted with an ACE Excel 5 C18-Amide column (250 mm × 4.6 mm). The mobile phase was 0.1% formic acid in water at a flow rate of 0.4 ml/min. Ammonium was quantified using the Ammonia Assay Kit AA0100 (Sigma-Aldrich). Three independent assays were performed in all cases.

The total amino acid content of the culture samples (free plus those forming polypeptides) was determined after an acid hydrolysis of the samples for 20 h at 110 °C in 6 M HCl, 0.1% phenol and 0.1% thioglycolic acid under reduced pressure in an argon atmosphere. Identification and quantification of the amino acids was performed by Alphalyse (Denmark) with a BioChrom 30 amino acid analyser using ion exchange chromatography, post-column derivatization with ninhydrin, and detection at 570 nm and 440 nm. A known amount of the amino acid sarcosine was added as an internal standard control. The 20 common amino acids, except for tryptophan and cysteine, were all determined in duplicate.

The redox potential of the cells was measured by collecting them from 1.5 ml of culture and treating them with 2,3,4-triphenyl-2H-tetrazolium chloride as previously described

(Defez *et al.,* 2017). pH was measured using a pH-meter. To determine the dry weight of culture samples, 50 ml of culture were centrifuged at 7000 × rpm for 10 min. The resulting pellets were dried for 24 h at 60 °C and weighed using an analytical balance.

Constraint-based analyses of metabolic fluxes

The most recent and complete genome-scale metabolic model of *P. putida* KT2440, *i*JN1411, was used for all metabolic flux estimations (Nogales *et al.,* 2017). *i*JN1411 includes 2826 metabolic and transport reactions, 2087 metabolites and 1411 genes, and provides the best available representation of *P. putida* metabolism. The model accounts for a large number of reactions mimicking the exchange with the environment of up to 337 different metabolites. *i*JN1411 is able to use 220 metabolites as the sole carbon and energy source, as well as 105 metabolites as the sole nitrogen source. In addition, *i*JN1411 can account for growth in rich media, such as LB (Nogales *et al.,* 2017). Flux balance analysis (FBA) (Varma and Palsson, 1995; Orth *et al.,* 2010) was used to make growth rate predictions and to determine initial flux distributions. FBA is based on solving linear optimisation problems by maximizing or minimizing a given objective function 'Z' subject to a set of constraints. The constraint 'S·v = 0' corresponds to a situation of steady-state mass conservation where the change in concentration of the metabolites as a function of time is zero. 'S' is an *m* x *n* matrix containing all the stoichiometric coefficients in the model of *m* metabolites and *n* reactions, and the vector 'v' has *n* elements that represent the individual flux values for each reaction. These fluxes are additionally constrained by the imposed lower and upper limits (bounds) 'vl' and 'vu'. The output is a flux distribution that maximizes or minimizes a given objective function. The growth rate was used routinely as the objective function. The output is a flux distribution that maximizes or minimizes a given objective function—in this case the growth rate. All computational simulations were performed using the COBRA toolbox (Schellenberger *et al.,* 2011) in the MATLAB environment (The MathWorks Inc.). Linear optimization problems were solved using the GNU Linear Programming Kit (GLPK) (http://www.gnu.org/software/glpk).

Construction of growth-phase condition-specific models

To simulate bacterial growth in LB, an initial *in silico* medium was defined based on the composition of LB and the reported gene analysis of strain KT2440 (Oh *et al.,* 2007; Molina-Henares *et al.,* 2010; Nogales *et al.,* 2017). The initial *in silico* LB composition was completed with the metabolites detected in the present analyses (Supporting Information Table S1). Thus, the default growth conditions for LB included the free uptake of those metabolites present in the medium, while allowing for the free exchange of CO_2, H_2O, H^+, HCO_3^-, Na^+, NH_4^+, Pi, Fe^{2+} and SO_4^{2-}. Constraint-based metabolic models calculate intracellular flux distributions that satisfy three fundamental types of constraints: steady-state mass-balance, reaction reversibility and flux capacities. For the latter, the flux measured for a given reaction, including nutrient uptake rates, can be imposed on the model, constraining the solution space. The growth-phase specific models were therefore constructed by constraining to experimental values the bounds of the exchange reactions corresponding to the different compounds for which uptake and/or secretion rates could be determined (sugars, organic acids, amino acids, lipids, nucleotides and ammonium) at each time point (Supporting Information Table S1). Specific models reproducing the growth rate and nutrient exchange during early, mid and late exponential growth could therefore be constructed.

Quantitative analysis of proteomes by mass spectrometry (MS) using isobaric tagging relative and absolute quantitation (iTRAQ)

Proteomic analyses were performed at the CNB-CSIC proteomics facility (Madrid, Spain; http://proteo.cnb.csic.es/proteomica/) using the iTRAQ procedure. Forty, twenty or ten millilitre of bacterial suspension obtained from cultures at a turbidity of 0.2, 0.6 or 2.0, respectively, were centrifuged for 5 min at 13,000 × *g* at 4 °C. The cell pellets were washed twice in 10 ml of 0.1 M PBS buffer (10 mM Na_2HPO_4, 2 mM KH_2PO_4, pH 7.4, 137 mM NaCl, 2.7 mM KCl) and stored at −80 °C. These frozen cell pellets were resuspended in 0.5 ml of 0.1 M PBS buffer pH 7 containing a cocktail of protease inhibitors (cOmplete™ Mini from Roche) and disrupted by sonication on ice. Cell debris was eliminated by centrifugation at 13,000 × *g* for 20 min at 4 °C. The protein concentration was determined using the Pierce™ BSA Protein Assay Kit (ThermoFisher Scientific). Proteins in the supernatant were precipitated with methanol/chloroform (Wessel and Flugge, 1984) and resuspended in 160 μl of a buffer containing 7 M urea, 2 M thiourea and 100 mM tetraethylammonium bromide. For iTRAQ tagging, 40 μg of proteins from two samples were digested overnight at 37 °C with 4 μg of trypsin (Sigma-Aldrich). The resulting peptides were labelled for 2 h with iTRAQ tags (AB Sciex; one tag for each sample, 6-plex procedure). The labelled samples were then mixed and cleaned by passage through a C18 SEP-PAK column. An amount of sample equivalent to a total of 1 μg of labelled peptides was analysed by liquid chromatography/mass spectrometry in an AB Sciex Triple Q-TOF mass spectrometer.

Protein identification and the analysis of protein differential expression were performed by Proteobotics S.L. (Madrid, Spain). Briefly, MS/MS spectra were exported to *mgf* format using Peak View v1.2.0.3 and examined, using Mascot Server 2.5.1, OMSSA 2.1.9, X!TANDEM 2013.02.01.1 and Myrimatch 2.2.140 software against a composite target/decoy database built from the 5313 *P. putida* KT2440 sequences held in the Uniprot Knowledgebase (November 2015), together with commonly occurring contaminants. Search engines were configured to match potential peptide candidates with a mass error tolerance of 25 ppm and a fragment ion tolerance of 0.02 Da. Up to two missed tryptic cleavage sites and a maximum isotope error (^{13}C) of 1 were allowed, contemplating fixed methyl-methane-thiosulphonate modification of cysteine and the variable oxidation of methionine, pyroglutamic acid derived from glutamine or glutamic acid at the peptide N-terminus, and the modification of lysine and the N-terminus by Tandem Mass Tags (TMT) 6-plex reagents. Score distribution models were used to compute peptide-spectrum match *p*-values (Ramos-Fernández *et al.,* 2008). Spectra for peptides recovered after filtering with a false discovery rate of ≤0.01 were selected for quantitative analysis. Approximately 1% of the signals of the lowest quality were removed. Differential regulation was measured using linear models (López-Serra *et al.,* 2014). Statistical significance was measured using *q*-values (FDR). All analyses were conducted using software from Proteobotics. Proteins showing an abundance change of ≥1.4 fold (log_2 fold change of 0.49) and a *q*-value of ≤0.05 were considered differentially expressed (Koul *et al.,* 2014).

Acknowledgements

We are grateful to L. Yuste for excellent technical assistance. This work was funded by grants BIO2015-66203-P to FR and BIO2014-59528-JIN to JN from Ministerio de Ciencia, Innovación y Universidades, Spain (AEI/FEDER, EU).

References

Adams, B.L. (2016) The next generation of synthetic biology chassis: moving synthetic biology from the laboratory to the field. *ACS Synth Biol* **5**: 1328–1330.

Aguilar-Uscanga, B., and Francois, J.M. (2003) A study of the yeast cell wall composition and structure in response to growth conditions and mode of cultivation. *Lett Appl Microbiol* **37**: 268–274.

Bauchop, T., and Eldsen, S.R. (1960) The growth of microorganisms in relation to their energy supply. *J Gen Microbiol* **23**: 457–569.

Belda, E., van Heck, R.G., José López-Sánchez, M., Cruveiller, S., Barbe, V., Fraser, C., *et al*. (2016) The revisited genome of *Pseudomonas putida* KT2440 enlightens its value as a robust metabolic chassis. *Environ Microbiol* **18**: 3403–3424.

Chubukov, V., Gerosa, L., Kochanowski, K., and Sauer, U. (2014) Coordination of microbial metabolism. *Nat Rev Microbiol* **12**: 327–340.

Crousilles, A., Dolan, S.K., Brear, P., Chirgadze, D.Y., and Welch, M. (2018) Gluconeogenic precursor availability regulates flux through the glyoxylate shunt in *Pseudomonas aeruginosa*. *J Biol Chem* **293**: 14260–14269.

Defez, R., Andreozzi, A., and Bianco, C. (2017) Quantification of triphenyl-2H-tetrazoliumchloride reduction activity in bacterial cells. *Bio-protocol* **7**: e2115.

Dvorak, P., and de Lorenzo, V. (2018) Refactoring the upper sugar metabolism of *Pseudomonas putida* for co-utilization of cellobiose, xylose, and glucose. *Metab Eng* **48**: 94–108.

Ebert, B.E., Kurth, F., Grund, M., Blank, L.M., and Schmid, A. (2011) Response of *Pseudomonas putida* KT2440 to increased NADH and ATP demand. *Appl Environ Microbiol* **77**: 6597–6605.

Escapa, I.F., García, J.L., Buhler, B., Blank, L.M., and Prieto, M.A. (2012) The polyhydroxyalkanoate metabolism controls carbon and energy spillage in *Pseudomonas putida*. *Environ Microbiol* **14**: 1049–1063.

Fedral-Register. (1982) *Appendix E, Certified Host-Vector Systems*, Vol. **47**, Bethesda, Maryland: NIH, p. 17197.

Franklin, F.C., Bagdasarian, M., Bagdasarian, M.M., and Timmis, K.N. (1981) Molecular and functional analysis of the TOL plasmid pWWO from *Pseudomonas putida* and cloning of genes for the entire regulated aromatic ring *meta* cleavage pathway. *Proc Natl Acad Sci U S A* **78**: 7458–7462.

Koul, A., Vranckx, L., Dhar, N., Gohlmann, H.W., Ozdemir, E., Neefs, J.M., *et al*. (2014) Delayed bactericidal response of *Mycobacterium tuberculosis* to bedaquiline involves remodelling of bacterial metabolism. *Nat Commun* **5**: 3369.

del Castillo, T., and Ramos, J.L. (2007) Simultaneous catabolite repression between glucose and toluene metabolism in *Pseudomonas putida* is channeled through different signaling pathways. *J Bacteriol* **189**: 6602–6610.

del Castillo, T., Ramos, J.L., Rodríguez-Hervá, J.J., Fuhrer, T., Sauer, U., and Duque, E. (2007) Convergent peripheral pathways catalyze initial glucose catabolism in *Pseudomonas putida*: genomic and flux analysis. *J Bacteriol* **189**: 5142–5152.

del Castillo, T., Duque, E., and Ramos, J.L. (2008) A set of activators and repressors control peripheral glucose pathways in *Pseudomonas putida* to yield a common central intermediate. *J Bacteriol* **190**: 2331–2339.

La Rosa, R., Behrends, V., Williams, H.D., Bundy, J.G., and Rojo, F. (2016) Influence of the Crc regulator on the hierarchical use of carbon sources from a complete medium in *Pseudomonas*. *Environ Microbiol* **18**: 807–818.

Lanning, M.C., and Cohen, S.S. (1951) The detection and estimation of 2-ketohexonic acids. *J Biol Chem* **189**: 109–114.

López-Serra, P., Marcilla, M., Villanueva, A., Ramos-Fernández, A., Palau, A., Leal, L., *et al*. (2014) A DERL3-associated defect in the degradation of SLC2A1 mediates the Warburg effect. *Nat Commun* **5**: 3608.

Matsushita, K., Shinagawa, E., Adachi, O., and Ameyama, M. (1979) Membrane-bound D-gluconate dehydrogenase from *Pseudomonas aeruginosa*. Its kinetic properties and a reconstitution of gluconate oxidase. *J Biochem* **86**: 249–256.

Molina-Henares, M.A., de la Torre, J., García-Salamanca, A., Molina-Henares, A.J., Herrera, M.C., Ramos, J.L., and Duque, E. (2010) Identification of conditionally essential genes for growth of *Pseudomonas putida* KT2440 on minimal medium through the screening of a genome-wide mutant library. *Environ Microbiol* **12**: 1468–1485.

Moreno, R., Martínez-Gomariz, M., Yuste, L., Gil, C., and Rojo, F. (2009) The *Pseudomonas putida* Crc global regulator controls the hierarchical assimilation of amino acids in a complete medium: evidence from proteomic and genomic analyses. *Proteomics* **9**: 2910–2928.

Moreno, R., Fonseca, P., and Rojo, F. (2012) Two small RNAs, CrcY and CrcZ, act in concert to sequester the Crc global regulator in *Pseudomonas putida*, modulating catabolite repression. *Mol Microbiol* **83**: 24–40.

Moreno, R., Hernández-Arranz, S., La Rosa, R., Yuste, L., Madhushani, A., Shingler, V., and Rojo, F. (2015) The Crc and Hfq proteins of *Pseudomonas putida* cooperate in catabolite repression and formation of ribonucleic acid complexes with specific target motifs. *Environ Microbiol* **17**: 105–118.

Nelson, K.E., Weinel, C., Paulsen, I.T., Dodson, R.J., Hilbert, H., Martins dos Santos, V.A., *et al*. (2002) Complete genome sequence and comparative analysis of the metabolically versatile *Pseudomonas putida* KT2440. *Environ Microbiol* **4**: 799–808.

Nikel, P.I., Martínez-García, E., and de Lorenzo, V. (2014) Biotechnological domestication of pseudomonads using synthetic biology. *Nat Rev Microbiol* **12**: 368–379.

Nikel, P.I., Chavarria, M., Fuhrer, T., Sauer, U., and de Lorenzo, V. (2015) *Pseudomonas putida* KT2440 strain metabolizes glucose through a cycle formed by enzymes of the Entner-Doudoroff, Embden-Meyerhof-Parnas, and pentose phosphate pathways. *J Biol Chem* **290**: 25920–25932.

Nogales, J., Palsson, B.O., and Thiele, I. (2008) A genome-scale metabolic reconstruction of *Pseudomonas putida* KT2440: *i*JN746 as a cell factory. *BMC Syst Biol* **2**: 79.

Nogales, J., Gudmundsson, S., Duque, E., Ramos, J.L., and Palsson, B.O. (2017) Expanding the computable reactome in *Pseudomonas putida* reveals metabolic cycles providing robustness. *bioRxiv* : 139121. https://doi.org/10.1101/139121.

Oh, Y.K., Palsson, B.O., Park, S.M., Schilling, C.H., and Mahadevan, R. (2007) Genome-scale reconstruction of metabolic network in *Bacillus subtilis* based on high-throughput phenotyping and gene essentiality data. *J Biol Chem* **282**: 28791–28799.

Orth, J.D., Thiele, I., and Palsson, B.O. (2010) What is flux balance analysis? *Nat Biotechnol* **28**: 245–248.

Plata, M.R., Koch, C., Wechselberger, P., Herwig, C., and Lendl, B. (2013) Determination of carbohydrates present in *Saccharomyces cerevisiae* using mid-infrared spectroscopy and partial least squares regression. *Anal Bioanal Chem* **405**: 8241–8250.

Poblete-Castro, I., Becker, J., Dohnt, K., Dos Santos, V.M., and Wittmann, C. (2012) Industrial biotechnology of *Pseudomonas putida* and related species. *Appl Microbiol Biotechnol* **93**: 2279–2290.

Puchalka, J., Oberhardt, M.A., Godinho, M., Bielecka, A., Regenhardt, D., Timmis, K.N., *et al*. (2008) Genome-scale reconstruction and analysis of the *Pseudomonas putida* KT2440 metabolic network facilitates applications in biotechnology. *PLoS Comput Biol* **4**: e1000210.

Ramos-Fernández, A., Paradela, A., Navajas, R., and Albar, J. P. (2008) Generalized method for probability-based peptide and protein identification from tandem mass spectrometry data and sequence database searching. *Mol Cell Proteomics* **7**: 1748–1754.

Rojo, F. (2010) Carbon catabolite repression in *Pseudomonas*: optimizing metabolic versatility and interactions with the environment. *FEMS Microbiol Rev* **34**: 658–684.

Sambrook, J., and Russell, D.W. (2001) *Molecular Cloning: A Laboratory Manual*. Cold Spring Harbor, N.Y.: Cold Spring Harbor Laboratory.

Sawyer, M.H., Baumann, P., Baumann, L., Berman, S.M., Canovas, J.L., and Berman, R.H. (1977) Pathways of D-fructose catabolism in species of pseudomonas. *Arch Microbiol* **112**: 49–55.

Schellenberger, J., Que, R., Fleming, R.M., Thiele, I., Orth, J.D., Feist, A.M., *et al*. (2011) Quantitative prediction of cellular metabolism with constraint-based models: the COBRA toolbox v2.0. *Nat Protoc* **6**: 1290–1307.

van Schie, B.J., Hellingwerf, K.J., van Dijken, J.P., Elferink, M.G., van Dijl, J.M., Kuenen, J.G., and Konings, W.N. (1985) Energy transduction by electron transfer via a pyrrolo-quinoline quinone-dependent glucose dehydrogenase in *Escherichia coli*, *Pseudomonas aeruginosa*, and *Acinetobacter calcoaceticus* (var. *lwoffi*). *J Bacteriol* **163**: 493–499.

Sezonov, G., Joseleau-Petit, D., and D'Ari, R. (2007) *Escherichia coli* physiology in Luria-Bertani broth. *J Bacteriol* **189**: 8746–8749.

Sonnleitner, E., Abdou, L., and Haas, D. (2009) Small RNA as global regulator of carbon catabolite repression in *Pseudomonas aeruginosa*. *Proc Natl Acad Sci U S A* **106**: 21866–21871.

Sonnleitner, E., Wulf, A., Campagne, S., Pei, X.Y., Wolfinger, M.T., Forlani, G., *et al*. (2018) Interplay between the catabolite repression control protein Crc, Hfq and RNA in Hfq-dependent translational regulation in *Pseudomonas aeruginosa*. *Nucleic Acids Res* **46**: 1470–1485.

Varma, A., and Palsson, B.O. (1995) Parametric sensitivity of stoichiometric flux balance models applied to wild-type *Escherichia coli* metabolism. *Biotechnol Bioeng* **45**: 69–79.

Ward, J.H., Jr. (1963) Hierarchical grouping to optimize an objective function. *J Am Stat Assoc* **58**: 236–244.

Wessel, D., and Flugge, U.I. (1984) A method for the quantitative recovery of protein in dilute solution in the presence of detergents and lipids. *Anal Biochem* **138**: 141–143.

Wittgens, A., Tiso, T., Arndt, T.T., Wenk, P., Hemmerich, J., Müller, C., *et al*. (2011) Growth independent rhamnolipid production from glucose using the non-pathogenic *Pseudomonas putida* KT2440. *Microb Cell Fact* **10**: 80.

Supporting Information

Additional Supporting Information may be found in the online version of this article at the publisher's web-site:

Figure S1. Concentration of free amino acids (black bars) and total amino acids (free + those in polypeptides; grey bars) in LB.

Figure S2. Growth (turbidity at 600 nm) of *P. putida* KT2440 in M9 minimal salts medium with 3 mM glucose

(Glc), 5 mM glutamate (Glu), 0.25% of starch, cellobiose, maltodextrin or mannan, or combinations of these polysaccharides with glucose or glutamate.

Figure S3. Predictions of metabolite fluxes for central carbon metabolism (**A**) and amino acid metabolism (**B**) during early exponential growth. The fluxes correspond to those predicted by the *i*JN1411 metabolic model constrained by the consumption data in Table S1. Fluxes >0.1 mmol/g cell dry weight/h are indicated in parentheses. Compounds predicted to be released to the medium are boxed in yellow.

Figure S4. Changes in central carbon metabolism at mid exponential growth compared to early exponential growth according to (**A**) the metabolic flux model, and (**B**) proteomic analysis. Arrows indicate fluxes (A) or proteins (B) that are more abundant (red), or less abundant (green), or do not change (black) with respect to the previous phase. Blue, reactions that do not occur in the initial phase, or that change direction. Arrow thickness is roughly proportional to the fluxes/changes observed. Dashed green lines indicate that some enzymes in the pathway are repressed. Fluxes >0.1 mmol/g cell dry weight/h are indicated in parentheses. Compounds predicted to be extruded are boxed in yellow; those that accumulate are boxed in blue. Reactions inverted (*) or nor observed (**) relative to the previous phase are indicated.

Figure S5. Changes in the metabolism of amino acids in mid exponential growth relative to early exponential growth according to (**A**) the metabolic flux model, and (**B**) proteomic analysis. Arrows indicate fluxes (A) or proteins (B) that are more abundant (red), or less abundant (green), or do not change (black), with respect to the previous phase. Arrow thickness is roughly proportional to the fluxes/changes observed. Reactions that do not occur in early exponential growth, or that change direction, are indicated in blue. Dashed green lines indicate that some enzymes in the pathway are repressed. Compounds predicted to be expelled, or accumulated, are boxed in yellow or blue, respectively. Reactions inverted (*) or nor observed (**) relative to the previous phase are indicated.

Figure S6. Changes in central carbon metabolism in late exponential growth relative to mid exponential growth according to (**A**) the metabolic flux model, and (**B**) proteomic analysis. Arrows indicate fluxes (A) or proteins (B) that are more abundant (red), or less abundant (green), or do not change (black). Arrow thickness is roughly proportional to the fluxes/changes observed. Reactions that do not occur in mid exponential growth, or that change direction, are indicated in blue. Violet, compounds detected but not included in the model. Dashed lines indicate that some enzymes in the pathway are activated (red) or repressed (green). Compounds predicted to be expelled are boxed in yellow. Compounds predicted to be expelled, or accumulated, are boxed in yellow or blue, respectively. Reactions inverted (*) or nor observed (**) relative to the previous phase are indicated.

Figure S7. Changes in the metabolism of amino acids in late exponential growth relative to mid exponential growth according to (**A**) the metabolic flux model, and (**B**) proteomic analysis. Arrows indicate fluxes (A) or proteins (B) that are more abundant (red), or less abundant (green), or do not change (black). Arrow thickness is roughly proportional to the fluxes/changes observed. Reactions that do not occur in mid exponential growth, or that change direction, are indicated in blue. Red dashed lines indicate that some enzymes in the pathway are activated. Compounds predicted to be expelled are boxed in yellow. Reactions inverted (*) or nor observed (**) relative to the previous phase are indicated.

Table S1. Composition of LB before (initial) and after inoculation with *P. putida* KT2440, during early (A_{600} = 0.2), mid (A_{600} = 0.6) and late exponential (A_{600} = 2) growth. The highest consumptions rates for each compound in each growth period are highlighted in grey. The values underlined were determined following predictions made by the flux model. Total glucose refers to free glucose plus that present in polysaccharides. N. d., not determined. (*) Data from reference (La Rosa *et al.,*); (**) TTC reduction assay ($A_{510\ nm}$ ml/mg of cell dry weight).

Table S2. Proteins showing increased or decreased abundance (change ≥1.4 fold; $\log_2$ of 0.49), and a *q*-value of ≤0.05 in mid exponential growth relative to early exponential growth (Excel sheet labelled 'Mid-vs-Initial'), or in late exponential growth relative to mid exponential growth (Excel sheet labelled 'Late-vs-Mid').